JCI insight

PI3Kgamma promotes neutrophil extracellular trap formation by noncanonical pyroptosis in abdominal aortic aneurysm

Yacheng Xiong, … , Baihong Pan, Wei Wang

JCI Insight. 2024. https://doi.org/10.1172/jci.insight.183237.

Research In-Press Preview

Graphical abstract

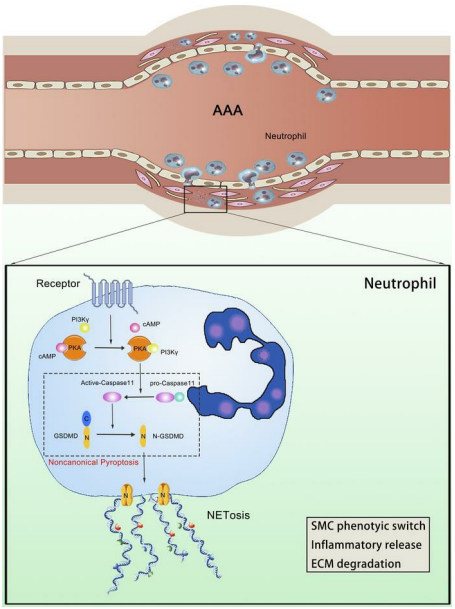

Find the latest version:

https://jci.me/183237/pdf

PI3Kgamma promotes neutrophil extracellular trap formation by noncanonical pyroptosis in abdominal aortic aneurysm

Contributing Authors:

Yacheng Xiong[1], PhD, yachengxiong@outlook.com.

Shuai Liu[1], PhD, liushuai@csu.edu.cn.

Yu Liu[1], PhD, liuyu18cn@163.com.

Jiani Zhao[1], MS, zhaojiani111@hotmail.com.

Jinjian Sun[1], PhD, jinjians@csu.edu.cn.

Yongqing Li[2], yqli@med.umich.edu

Baihong Pan[1, *], PhD, pbh1990s@csu.edu.cn.

Wei Wang[1,3, *], PhD, weiwangcsu@csu.edu.cn.

Affiliations:

1 Department of General & Vascular Surgery, Xiangya Hospital, Central South University, Changsha 410008, China

2 Department of Surgery, University of Michigan Health System, Ann Arbor, MI, United States

3 National Clinical Research Center for Geriatric Disorders, Xiangya Hospital, Central South University, Changsha 410008, China

***Correspondence to**:

Wei Wang: weiwangcsu@csu.edu.cn; Baihong Pan: pbh1990s@126.com

Address correspondence to: General &Vascular Surgery, Xiangya Hospital, Central South University, 87#, Xiangya Road, Changsha 410008, Hunan Province, China

Tel: +86 073189753008

Declaration of interests

The authors declare no competing interests.

Abstract

Abdominal aortic aneurysm (AAA) is one of the most life-threatening cardiovascular diseases; however, effective drug treatments are still lacking. The formation of neutrophil extracellular traps (NETs) has been shown to be crucial trigger of AAA and identifying upstream regulatory targets is thus key to discovering therapeutic agents for AAA. We revealed that phosphoinositide 3-kinase gamma (PI3Kγ) acted as an upstream regulatory molecule, and that PI3Kγ inhibition reduced NET formation and aortic wall inflammation, thereby markedly ameliorating AAA. However, the mechanism of NET formation regulated by PI3Kγ remains unclear. In this study, we showed that PI3Kγ deficiency inactivated the noncanonical pyroptosis pathway, which suppressed downstream NET formation. In addition, PI3Kγ regulation of noncanonical pyroptosis was dependent on cAMP/protein kinase A (cAMP/PKA) signaling. These results clarify the molecular mechanism and crosstalk between PI3Kγ and NETosis in the development of AAA, potentially facilitating the discovery of therapeutic options for AAA.

Keywords: PI3Kgamma; Neutrophil extracellular trap; Noncanonical pyroptosis; cAMP/PKA; Abdominal aortic aneurysm

Introduction

Abdominal aortic aneurysm (AAA) is a balloon-like bulge in the abdominal segment of the aortic wall, caused by various factors, and its rupture is a major cause of death in adults (1). The prevalence of AAA is up to 0.92% in people aged 30-79 worldwide (2). Progressive aneurysm dilatation eventually progresses to aneurysm rupture, with a mortality rate of more than 81% (3). To date, there is no effective drug treatment to prevent the formation and growth of aneurysms (4), and existing drugs used in clinical trials for the treatment of AAA have not yet shown good efficacy (5). There is thus an urgent need to explore the potential mechanisms responsible for AAA and to discover effective therapies.

Inflammation plays a pivotal role in the pathological process of AAA (6). Varieties immune cells, including neutrophils, monocytes/macrophages, eosinophils, and lymphocytes, infiltrate the arterial wall tissue, associated with the development of AAA (7). Among these inflammatory cells, neutrophils are recruited to the inflammatory vessel wall at an early stage of AAA formation (8). A prospective cohort study showed a strong positive association between neutrophil count and AAA development, independent of other traditional risk factors, such as smoking, obesity, and atherosclerosis (9). Limiting neutrophil recruitment to the arterial wall reduced the incidence of elastase-perfusion AAA (10), and inhibition of neutrophils using anti-neutrophil antibodies also limits the progression of experimental AAA (8). In addition, neutrophil-derived biomarkers may be of clinical value for the monitoring and prognosis of AAA and may be used to guide early therapeutic interventions (11),

suggesting that neutrophils may be a therapeutic target in AAA. The application of neutrophil-neutralizing antibodies to reduce neutrophils in the treatment of AAA however, has only a short-term effect and damages the host's innate immune defense function (12). Elucidating the mechanism of neutrophils promoting AAA is therefore important for the discovering of therapeutic drug targets.

Neutrophils play an important role in immune defense through phagocytosis, degranulation, and the formation of neutrophil extracellular traps (NETs) (13). NETs are composed of depolymerized chromatin, citrullinated histone 3 (Cit H3), granule proteins, and cytoplasmic proteins (14). NET formation contributes to pathogen clearance; however, uncontrolled NET formation accelerates the deterioration of sterile inflammatory diseases, including atherosclerosis (15). Previous studies showed that circulating NETs were strongly correlated with the severity of AAA (16), and that NETs aggregated AAA via the initiation and promotion of inflammatory responses, smooth muscle phenotype switching, and extracellular matrix degradation through matrix metalloproteinases (MMPs) (17-19). A further study proved that reducing NET formation in the abdominal aorta markedly protected against elastase-induced AAA (20). Blockage of NET formation is currently achieved through inhibition of peptidyl arginine deiminases (PADs), which are expressed in neutrophils and drive histone citrullination (21). Notably however, PAD-deficient mice exhibited innate immune dysfunction and were more susceptible to bacterial infections (22), indicating the need to identify another possible trigger of NETs for the development of therapeutic agents for AAA (23).

Phosphoinositide 3-kinase gamma (PI3Kγ) belongs to the PI3K protein family, which is mainly expressed in immune cells and is involved in the progression of inflammatory-related diseases. Blocking PI3Kγ is accordingly regarded as an effective strategy for the treatment of inflammatory diseases (24). Thiago et al. reported that the release of NETs from human neutrophils was dependent on the activation of PI3Kγ during Leishmania infection (25). A recent study also revealed that PI3Kγ inhibition could reduce NET formation in the treatment of microscopic polyarteritis (26), suggesting that PI3Kγ may be an upstream regulator of NET formation. However, the role of PI3Kγ in AAA progression via promoting NET formation remains unclear, and the mechanism by which PI3Kγ regulates NETs is still poorly understood.

Herein, we revealed that PI3Kγ inhibition reduced neutrophil infiltration and NET formation in the arterial wall of AAA. Reduction of NET formation by PI3Kγ blockade was achieved by restraining the noncanonical pyroptosis pathway, and PI3Kγ regulated this pathway via the cAMP/PKA signaling. We clearly demonstrated that PI3Kγ regulated the progression of AAA via a mechanism involving PI3Kγ–cAMP/PKA–noncanonical pyroptosis–NETosis. The results of this study provide an insight into the prevention of AAA and broaden our understanding of the upstream regulatory sites of NET formation.

Results

Neutrophil infiltration and NET formation were upregulated in human and mouse AAA tissues

To reveal levels of NET formation in the AAA wall, we quantified NETs in human AAA samples and control adjacent abdominal aortic tissue (adjacent AA). Expression levels of CitH3 protein, as a marker of NETs, were markedly upregulated in AAA tissues (Figure 1A). Additionally, we constructed PPE-induced AAA and quantified the timing of NET formation, protein from abdominal aortas was collected at 0, 3, 7, and 14 days after elastase perfusion. CitH3 expression peaked in aortas from days 3–7 and was downregulated at day 14 (Figure 1B). Furthermore, we performed immunofluorescence staining to verified the change of NETs expression, the results revealed increased NET expression in AAA tissues (Figure 1C and 1D). To further reveal neutrophil infiltration in AAA, neutrophils (Ly6G+) were evaluated by immunohistochemistry and showed neutrophil infiltration was increased in aortas from AAA compared with saline-treated mice (Figure S2A). These results suggest that abnormal neutrophil infiltration and NET expression were closely associated with AAA.

Inhibition of NETs alleviated elastase-induced AAA in mice

To reveal the crucial effect of NET formation in AAA development, we examined the effect of Cl-amidine (A PAD4 inhibitor, blocking NET formation) on PPE-induced AAA (Figure 2A). Ultrasonography of the abdominal aorta demonstrated smaller aorta lumen diameters in the Cl-amidine group compared with the vehicle (saline) group from

days 7–14 after PPE surgery (Figure 2B). There were also significant differences in the external diameter of the aorta between the Cl-amidine and vehicle groups (Figure 2C). Histomorphology showed that the degradation of elastin in the Cl-amidine group was less destroyed than in the control group (Figure 2D). To verify the inhibitory effect of Cl-amidine, we carried out immunofluorescence staining of NETs in the aorta, and showed that NET expression was markedly decreased after Cl-amidine administration (Figure 2E). In addition, CitH3 protein expression was significantly reduced at any time point after PPE surgery in Cl-amidine-treated mice (Figure 2F). Previous studies showed that NETs exacerbated AAA by promoting smooth muscle phenotypic switching, inflammatory release, and matrix degradation (19). We observed similar results. mRNA levels of the vascular smooth muscle (VSMC) contractile genes *Tagln*, *Cnn1*, *Acta2*, and *Myh11* were increased while the synthetic genes *Klf4* and *Spp1* were reduced in the Cl-amidine group. In addition, the proinflammatory genes *IL6*, *TNFa*, *Ccl2*, and *IL-1β* and the matrix metalloproteinase genes *MMP2* and *MMP9* were significantly decreased in the abdominal aorta of Cl-amidine-treated mice compared with control mice (Figure 2G). These data indicate that blocking the formation of NETs effectively inhibited the progression of AAA.

PI3Kγ knockout reduced neutrophil infiltration and NETs release in AAA

Given that inhibition of PAD impairs the innate immune defense system (22), we explored upstream regulatory factors of NET formation. PI3Kγ is involved in the regulation of neutrophil function (27), and we speculated that PI3Kγ might participate

in the development of AAA via inducing neutrophil NET formation. We therefore generated PI3Kγ knockout mice (*PI3Kγ*$^{-/-}$) (Figure S1A and S1B). PI3Kγ protein expression level was significantly increased in the abdominal aorta in WT mice on day 14 after elastase perfusion compared with day 0 (Figure S1C). To further elucidate the impact of PI3Kγ on AAA, we induced AAA in *PI3Kγ*$^{-/-}$ and WT mice and showed that PI3Kγ deficiency alleviate PPE-induced AAA, similar to Cl-amidine administration. Ultrasonography, gross morphology, and elastic Van Gieson staining of the abdominal aorta demonstrated that *PI3Kγ*$^{-/-}$ mice had less destroyed aortas compared with WT mice (Figure 3A–3B and Figure S2B). These results suggested that PI3Kγ was an important etiological factor of AAA. Meanwhile, neutrophil infiltration and NET formation were reduced in the *PI3Kγ*$^{-/-}$ group compared with the WT group (Figure 3C-3D) and CitH3 protein expression was significantly lower in *PI3Kγ*$^{-/-}$ compared with WT mice (Figure 3E). These results suggested that PI3Kγ acted as an upstream regulatory molecule of NET formation.

We further determined the downstream signals of NETs by real-time quantitative PCR. There were no significant differences in the VSMC markers *Cnn1*, *Acta2*, and *Klf4* between the WT and *PI3Kγ*$^{-/-}$ groups; however, there were significant differences in *Tagln*, *Myh11*, and *Spp1* between the two groups. The inflammatory genes, *IL6*, *TNFa*, *Ccl2*, *IL-1β* were significantly downregulated in *PI3Kγ*$^{-/-}$ mice, and MMP9, but not MMP2, expression levels were also reduced in PI3Kγ-/- mice (Figure S2C). All these results suggest that PI3Kγ blockade may alleviate the development of AAA by reducing the formation of NETs.

Deficiency of PI3Kγ inhibits NETs formation in neutrophil

To clarify the causal relationship between PI3Kγ and NET formation in neutrophils, we isolated and purified neutrophils (purity > 90%) from mice (Figure S3A-S3C), and stimulated them with LPS, as a classical inducer of NETs (28). The most appropriate concentration of LPS to induce NET was 5 μg/mL (Figure S3D). LPS-treated neutrophils from WT mice formed large amounts of NETs, and LPS-induced NET formation was significantly inhibited by the PI3Kγ inhibitor (IPI549) (Figure S4A-S4B). We also to mimicked the inflammatory state of AAA by stimulation of isolated neutrophils with TNFa. NET formation was significantly increased by TNFa, but was reversed after IPI549 administration (Figure S4C-S4D). We further corroborated the experimental results, by repeating most of the above experiments in neutrophils purified from *PI3Kγ*$^{-/-}$ and WT mice, and showed consistent results with those following PI3Kγ inhibitor treatment (Figure 4A-4D). All these results suggested that inhibition of PI3Kγ in neutrophils could reduce NET formation in vitro.

PI3Kγ expression in neutrophils was required for NET formation and AAA progression in mice

To further reveal the role of PI3Kγ from neutrophils in AAA formation, we generated elastase-induced AAA in *PI3Kγ*$^{-/-}$ mice. Neutrophils from WT mice are the only source of PI3Kγ in *PI3Kγ*$^{-/-}$ mice, and we therefore performed adoptive transfer of neutrophils isolated from WT mice into *PI3Kγ*$^{-/-}$ mice. A schematic diagram of the process is shown

in Figure 5A. *PI3Kγ*$^{-/-}$ mice that received WT neutrophils exhibited more severe AAA lesions compared with *PI3Kγ*$^{-/-}$ mice without neutrophil transfer. Both the maximal lumen and external diameters of the abdominal aorta were significantly greater in neutrophil-transferred *PI3Kγ*$^{-/-}$ mice than in vehicle-treated *PI3Kγ*$^{-/-}$mice (Figure 5B–5C). VVG staining of the abdominal aorta showed more severe elastin degradation in neutrophil-transferred *PI3Kγ*$^{-/-}$ mice (Figure 5D). We also evaluated NET formation by immunofluorescence and western blot, and showed that NET expression was significantly increased in neutrophil-transferred *PI3Kγ*$^{-/-}$ compared with vehicle-treated *PI3Kγ*$^{-/-}$ mice (Figure 5E-5F). Furthermore, adoptive transfer of neutrophils significantly decreased the expression of the VSMC contractile genes *Acta2*, *Cnn1*, *Tagln*, and *Myh11*, and significantly increased the expression of genes associated with the synthetic and inflammatory phenotype and extracellular matrix degradation (Figure 5G). These results suggest that neutrophil-derived PI3Kγ acted as a key regulatory molecule in NET formation in a mouse model of PPE-induced AAA.

PI3Kγ promoted NET formation via noncanonical pyroptosis pathways in vitro.

The above results suggested that inhibition of PI3Kγ alleviated AAA through suppressing NETosis. We therefore investigated the molecular mechanism by which PI3Kγ regulated NET formation. Previous studies identified ROS as a critical factor in the induction of NET formation (29). We therefore detected the protein expression of NADPH oxidase 2 (NOX2, a key enzyme in inducing ROS production) by western blot. LPS-treated neutrophils released large amounts of NETs, whereas PI3Kγ inhibition or

administration of the specific NOX inhibitor, DPI, significantly reduced NET formation, with an obvious synergistic effect. Interestingly however, PI3Kγ blockage had no effect on NOX2 protein expression (Figure S5A–S5B). These results suggest that the inhibitory effect of PI3Kγ deficiency on NET formation in neutrophils was independent of ROS signaling.

Previous studies also suggested that pyroptosis may be involved in the formation of NETs (30). We therefore measured the expression levels of gasdermin D (GSDMD, a key protein in the pyroptosis signaling pathway). Protein levels of N-GSDMD, the active splicing form of GSDMD, were significantly increased in human AAA compared with adjacent abdominal aorta tissue (Figure S6A). WT mouse neutrophils were isolated and treated with LPS. LPS treatment significantly increased N-GSDMD and CitH3 protein levels, and these effects were reversed by the specific GSDMD inhibitor DSF (Figure 6A). These results indicate that pyroptosis may be a key upstream regulatory signal for NET formation.

To investigate if PI3Kγ regulated NET formation via the pyroptosis pathway, we examined the expression of pyroptosis pathway-related proteins in WT and *PI3Kγ*$^{-/-}$ neutrophils. IL-1β and N-GSDMD expression levels were significantly inhibited in PI3Kγ-deficient mice (Figure 6B). These findings suggested that pyroptosis was a key bridge for PI3Kγ to promote NET formation. Previous studies showed that the occurrence of pyroptosis depends on the activation of canonical or noncanonical inflammatory pathway (31). We therefore examined the involvement of canonical and noncanonical inflammatory pathways in PI3Kγ-induced NET formation. To activate

canonical inflammatory pathway, neutrophils from WT or *PI3Kγ*$^{-/-}$ mice were primed with LPS followed by administration of nigericin to activate NLRP3 inflammasomes (caspase1), while noncanonical inflammatory pathways were activated using the TLR1/2 agonist Pam3CSK4 to suppress basal apoptosis, followed by LPS transfection into the neutrophil cytosol to activate caspase 11. Both canonical and noncanonical inflammasome activation significantly increased CitH3 expression and IL-1β release; however, only caspase 11/GSDMD signaling (noncanonical pyroptosis pathway) was inhibited after PI3Kγ blockade, whereas there was no significant difference in canonical pyroptosis pathway-associated proteins (caspase 1/IL-1β) between the PI3Kγ-/- and WT groups (Figure 6C). We then repeated the above experiment in neutrophils isolated from WT mice using a PI3Kγ inhibitor (IPI549) and showed that the results were consistent with those from PI3Kγ-derived neutrophils (Figure S6C). These results suggested that PI3Kγ might promote NET formation via noncanonical pyroptosis pathways.

We then explored the molecular mechanism by which blocking PI3Kγ inhibited the nonclassical pyroptosis pathway. The most common pathway is one by which PI3Kγ may directly regulate PI3K/Akt signaling through its lipid kinase function, which is thought to be directly downstream of PI3Kγ. We therefore detected NET expression after treatment with the specific Akt agonist SC79. PI3Kγ blockade reduced Akt phosphorylation and NET formation. Interestingly, phosphorylation of Akt was increased but CitH3 expression was decreased after SC79 treatment (Figure S7A–S7B). These results suggested that PI3Kγ regulated noncanonical pyroptosis independent of

Akt, indicating an alternative signal pathway. PI3Kγ can function as an anchor protein (32) for PKA to regulate the cAMP/PKA signaling pathway in a negative feedback loop (33). We speculated that PKA signaling might be involved in PI3Kγ-mediated regulation of the noncanonical pyroptosis pathway. We therefore blocked PKA signaling using a PKA inhibitor, H89, and an adenylyl cyclase inhibitor/cAMP product inhibitor, MDL12330A. Decreased NET expression by PI3Kγ blockade was counteracted by H89 or MDL12330A (Figure 6D). We further evaluated the cAMP/PKA signaling pathway by enzyme-linked immunosorbent assay and kinase activity assays. PI3Kγ inhibition reversed LPS-induced activation of cAMP/PKA signaling, while H89 and MDL12330A attenuated these processes (Figure 6E-6F). Concomitantly, western blot analysis shows that PI3Kγ deficiency deactivated the LPS-induced caspase 11/GSDMD signaling pathway. Notably, PI3Kγ-mediated inhibition of noncanonical pyroptosis in neutrophils was markedly reversed by pre-treatment with H89 or MDL12330A (Figure 6G). Similarly, these results were recapitulated in IPI549-treated neutrophils from WT mice (Figure S8A–S8B). Together, these data indicate that PI3Kγ may regulate noncanonical pyroptosis through the cAMP/PKA signaling pathway.

cAMP/PKA inhibitor eliminated the protective effect of PI3Kγ knockout in elastase-induced AAA

To investigate the possible involvement of cAMP/PKA signaling in AAA, *PI3Kγ*$^{-/-}$ mice received PPE-induced AAA and H89. H89 treatment significantly increased the AAA

size compared with vehicle treatment (Figure 7A–7C), and elastin fragmentation in the aortic wall was more severe in the H89 group compared with the vehicle group (Figure 7D). In addition, H89 significantly decreased the mRNA levels of *Acta2*, *Cnn1*, *Tagln*, and *Myh11* in the abdominal aorta and increased the mRNA levels of *Klf4*, as well as *IL6*, *TNFa*, *Ccl2*, *IL-1β*, and *MMP2* (Figure 7E). Additionally, We detected the cAMP concentration and PKA activity. H89 treatment significantly inhibited PKA kinase activity, with no obvious increase in cAMP levels (Figure 7F-7G). Immunofluorescence and western blot results showed a significant increase in the expression of NETs following H89 administration, compared with the vehicle group (Figure 7H-7I). Moreover, H89 aggravated caspase 11 activation and GSDMD cleavage in the arterial wall of *PI3Kγ*$^{-/-}$ mice (Figure 7I). These results suggested that PI3Kγ deficiency suppressed noncanonical pyroptosis and thus inhibited NET formation in a cAMP/PKA-dependent manner.

Discussion

Robust infiltration of inflammatory cells plays a critical role in the pathogenesis of AAA. Among of them, NETs derived from neutrophils are a key trigger inducing AAA dilation(6). Targeting NET formation may thus represent an avenue for treating AAA. Here we revealed that PI3Kγ, as the upstream regulatory molecule of NETs formation, may be a potential target for inhibiting AAA progression. Meanwhile, we elucidated that the molecular mechanism by which PI3Kγ regulated NET release was dependent on noncanonical pyroptosis. These findings provide a theoretical basis for targeting PI3Kγ to reduce arterial wall inflammation and treat AAA.

A previous study found that NETs induced VSMC apoptosis through p38/JNK signaling, degraded elastic fibers, and promoted angiotensin II-induced AAA (34). Another recent study showed that circulating NETs were positively correlated with clinical outcomes of AAA; NETs promoted VSMC inflammatory release and phenotypic transformation through Hippo-Yap signaling activation, exacerbating AAA dilation (17). These publications suggest that NETs play a critical role in promoting AAA progression. We also found a markedly increase in NET formation in human AAA and elastase-induced AAA, consistent with these previous findings. We further determined the expression of NETs at different time points in a mouse model of elastase-induced AAA, and showed that NETs peaked at days 3-7, and then decreased by day 14 after PPE surgery. This was consistent with previous studies (35, 36) showing that neutrophils were the initiating cells of the inflammatory response, and infiltration of the arterial wall occurred in the early stage of aneurysm formation, which may explain the decrease in

NETs in the late stage of aneurysm.

To date, studies on NET formation and aneurysms remain scarce. Although several studies have revealed a causal relationship between NETs and AAA (17, 34, 37), they mainly focused on the downstream mechanism by which NETs promoted AAA formation, while upstream regulatory mechanisms of NETs formation were rarely discussed which may provide a key target for therapeutic drug discovery. A recent study reported that treatment with the PAD4 inhibitor GSK484 inhibited NET formation and attenuated Ang II-induced experimental aneurysm progression (16). We subsequently investigated the protective effect of the specific PAD4 inhibitor Cl-amidine on aneurysms, and the results were consistent with previous studies (20), suggesting that NET formation played a crucial role in AAA formation. Unfortunately, the application of PAD inhibitors targeting NET formation will damage the innate immune function (22). and they are thus not suitable for prolonged administration for the treatment of AAA. It is therefore essential to identify upstream regulators of NETs for AAA treatment. Previous studies showed that inhibition of PI3Kγ promoted neutrophil senescence and reduced NETs, which in turn improved acute lung injury (38). In addition, PI3Kγ depletion protected against microscopic polyangiitis by inhibiting NET formation (26). We hypothesized that PI3Kγ may be involved in AAA progression by affecting NET formation. We accordingly showed that PI3Kγ was markedly upregulated in elastase-induced AAA mice, and PI3Kγ knockout markedly inhibited the formation of AAA. Furthermore, PI3Kγ blockade dramatically suppressed neutrophil infiltration and NET formation, inhibiting AAA formation. These results suggest that

PI3Kγ may be an upstream regulatory molecule of NETs in AAA formation and progression.

Although we used PI3Kγ global knockout mice to demonstrate a protective effect of PI3Kγ in AAA, it is difficult to explain that PI3Kγ of neutrophils plays a key role in AAA progression. PI3Kγ is widely expressed in many inflammatory cell types (39). Previous studies suggested that PI3Kγ promoted carotid re-endothelialization and aggravated vascular stenosis through Cxcl10 secretion by Th1 cells (40). PI3Kγ facilitated LDL uptake in macrophages to form foam cells and exacerbated atherosclerotic plaque formation (41). Therefore, PI3Kγ may also promote the release of NETs and aggravate AAA through other inflammatory cells. To clarify whether it is neutrophil-derived PI3Kγ that regulates NETs release and promotes AAA, we isolated neutrophils from mouse bone marrow and showed that inhibition of PI3Kγ reduced NET release, consistent with previous studies (42). Subsequently, we adoptively transferred bone marrow neutrophils from WT mice to PI3Kγ-/- mice to clarify the contribution of PI3Kγ in neutrophils to elastase-induced AAA, and showed that adoptively transferred WT neutrophils markedly worsened AAA in PI3Kγ-/- mice, confirming the involvement of neutrophil-derived PI3Kγ in aneurysms.

Despite the fact that PI3Kγ is involved in regulating NET formation during AAA, the molecular mechanism is still poorly understood. Previous studies identified ROS as an important inducer regulating the formation of NETs (43), and NOX2 as a key enzyme that produces ROS to mediate the formation of NETs (44). However, our data showed that PI3Kγ blockade reduced the expression of NETs, but did not decrease the

upregulation of NOX2 upon LPS stimulation, and had a synergistic effect when combined with a NOX2 inhibitor. This suggested that PI3Kγ regulated NET expression independent of ROS signaling pathways. Recent studies showed that GSDMD, as a key executioner of pyroptosis, was required for the formation of NETs (30). Cleaved GSDMD enhanced nuclear membrane permeability at the early stage of NET formation, thus facilitating the entry of cytoplasmic granules into the nucleus followed by pore formation at the cytoplasmic membrane to promote NET complex release (45), indicating that NETs formation was closely related to pyroptosis. The FDA-approved drug DSF, which is used to treat alcohol addiction, was recently shown to inhibit GSDMD pore formation (46). We found that LPS-induced NET formation was markedly reduced after DSF administration, consistent with previous studies (47). We therefore hypothesized that PI3Kγ regulated NET expression through pyroptosis. Accordingly, pyroptosis-related N-GSDMD was markedly increased in human AAA, confirming the clinical relevance of pyroptosis in AAA. In addition, pyroptosis signaling was markedly reduced under PI3Kγ deficiency, revealing its involvement in the regulation of pyroptosis. This provides a report of a link between PI3Kγ and pyroptosis.

Notably however, the mechanistic insight into the effects of PI3Kγ on pyroptosis are poorly understand. Previous studies showed that the induction of pyroptosis could be mediated by canonical and noncanonical pyroptosis pathways. Canonical pyroptosis results from the activation of caspase 1 by the inflammatory complex, whereas noncanonical pyroptosis results from the activation of caspase 11 by intracellular

LPS(31). We therefore induced canonical and noncanonical pyroptosis using LPS followed by nigericin stimulation, and Pam3CSK4 followed by LPS transfection, respectively, according to the previous publications (48). PI3Kγ deficiency reduced the formation of NETs and inhibited the activation of noncanonical pyroptosis and the release of IL-1β but had no effect on the canonical pyroptosis pathway. These results suggest that PI3Kγ regulates NET formation via noncanonical pyroptosis.

We further explored the mechanism by which PI3Kγ regulates noncanonical pyroptosis. PI3Kγ has phosphoinositide kinase activity which phosphorylates phosphatidylinositol 2 phosphate to phosphatidylinositol 3 phosphate, leading to the recruitment of Akt with a PH structural domain and activation of downstream signaling. Previous studies indicated that PI3Kγ-driven NET formation was dependent on the activation of Akt signaling (38, 42). However, they did not perform rescue experiments to prove that PI3Kγ regulated NET formation through PI3K/Akt. Our results suggested that PI3Kγ blockade reduced NET formation was accompanied by inhibition of AKT signaling, consistent with previous results. In contrast, when Akt signaling was markedly activated by SC79, NET levels were further reduced, implying that blocking PI3Kγ and Akt activation could synergisticslly suppress NET formation. A recent study suggested that activation of AKT/mTOR autophagy pathway promoted the transformation of neutrophil function from NETosis to phagocytosis (49). This may explain the protective effect on NETs formation after Akt signaling activation. The above results indicated that PI3Kγ regulated NETs in a manner independent of Akt signaling.

Patrucco et al. found that PI3Kγ, in addition to phosphatidyl kinase activity, acted as an

anchoring protein with a bridging function, negatively regulating cardiac contractility (50). PI3Kγ promoted the interaction of PKA with phosphodiesterase (PDEs) and negatively regulated cAMP/PKA signaling (51). We thus hypothesized that PI3Kγ regulated neutrophil noncanonical pyroptosis through cAMP/PKA signaling. We accordingly showed that the cAMP/PKA signaling, which was activated by PI3Kγ deletion, was re-suppressed in neutrophils after treatment with H89 and MDL12330A, and the protective effect of PI3Kγ deletion on NET formation was abolished. Additionally, the inhibitory effect of PI3Kγ deficiency on noncanonical pyroptosis signaling was also reversed after H89 and MDL12330A administration. We further explored the role of cAMP/PKA signaling in PI3Kγ-mediated AAA within elastase-induced AAA, and showed that blocking PKA signaling abrogated the protective effect of PI3Kγ deficiency on AAA, while NETs formation and noncanonical pyroptosis signaling in the arterial wall were also markedly enhanced. These results explain the molecular mechanism by which PI3Kγ regulates noncanonical pyroptosis-mediated NET formation in AAA.

This study had certain limitations. One limiatation is that although we have showed that PI3Kγ inhibition reduced NET formation, the precise molecular mechanism of NET formation remains unclear. Several different stimuli-specific signaling pathways are involved in NETosis, and further investigations should be performed to determine the potential crosstalk between the various upstream signaling pathways of NETosis, especially in AAA. The second limitation is that our goal of this study is to elucidate role of neutrophilic PI3Kγ on AAA development while PI3Kγ global KO mice was

applied in this experiment; neutrophil specific PI3Kγ KO is more suitable although neutrophil transfer experiment can support our conclusion. The third limitation is that previous studies have shown that endothelial PI3Kγ deficiency reduced neutrophil infiltration (52), which suggested that PI3Kγ derived from other cells may also play important functions in AAA. Therefore, neutrophil or endothelial specific PI3Kγ KO model should to be further investigated to enrich the functions of PI3Kγ in AAA developmentIn conclusion, our results revealed the molecular mechanism by which PI3Kγ regulates NET formation. We showed that PI3Kγ blockade markedly inhibited neutrophil infiltration and NET formation in the abdominal aorta, notably ameliorating multiple pathological changes in AAA. Previous studies have reported serious adverse events of current FDA-approved PI3K inhibitors (53), which may compromise its clinical usage. However, our study demonstrates that the PI3Kγ specific inhibition or downstream signaling pathway (for example NETosis) may be a therapeutic target for AAA treatment with less side effects. The results of this study may thus promote PI3Kγ specific inhibitors as potentially useful candidate drugs for the treatment of AAA.

Methods

Sex as a biological variable

Human aorta sample were collected. Male and female were involved. AAA animal model was performed and only male mice were used. Sex was not considered as a biological variable

reagents

The key reagents used in this experiment are shown in Table S1

Study design, subject recruitment, and sample collection

In the present study, patients with AAA were recruited at Xiangya Hospital (Changsha, China) from September 2021 to October 2022. AAA was confirmed by computed tomography angiography according to the 2018 American Society for Vascular Surgery (ASVS) guidelines for the diagnosis and treatment of AAA (54). AAA samples were collected from patients receiving open aneurysm repair. Control tissue samples were derived from adjacent, relatively normal abdominal aorta tissue. The demographic and clinical details of the patients are shown in Table S2. All included subjects provided written informed consent.

Animal study

Male wild-type (WT) specific pathogen-free (SPF) C57BL/6J mice aged 8 weeks were purchased from SPF Hunan SJA Laboratory Animal Co., Ltd. (Changsha, China).

PI3Kγ knockout mice (*PI3Kγ*$^{-/-}$) were purchased from GemPharmatech Co. Ltd. (Nanjing, China). The construction strategy and genotype identification are shown in Figure S1A and S1B.

The porcine pancreatic elastase (PPE)-induced AAA model was established by intravascular PPE perfusion as described previously (55). Briefly, mice were anesthetized with 1.5% isoflurane and PPE (4.0 U/mL dissolved in sterile saline) was delivered into the infrarenal aorta for 5min at 150 mmHg. Control mice underwent sham surgery and were administered an identical volume of saline.

Cl-amidine (20 mg/kg) and H89 (2 mg/kg) were administered by intraperitoneal injection in PPE-induced AAA model mice at different endpoints.

Neutrophil adoptive transfer mice were established by tail vein injection of neutrophils (10^6/mouse) once a day on days 2-3 after creation of the PPE models, as described previously (20). The AAA model was established in PI3Kγ KO mice. The experimental group mice were injected with neutrophils from WT mice, and the control group mice was injected with neutrophils from PI3Kγ KO mice. The number of neutrophils injected was consistent.

All AAA model mice were sacrificed for measurement of the maximal aortic diameter and tissue collection on day 14 after surgery. All animals were housed in SPF conditions at 23±1 ℃ and 50%-60% humidity in a 12-h light/dark cycle and were provided with a standard chow diet and water *ad libitum*.

Blood count

Mouse blood samples were collected and analyzed using an automated hematology analyzer (BC2800vet, Mindray) (Figure S1D).

Enzyme-Linked Immunosorbent Assay (ELISA)

Mouse blood samples were collected and centrifuged at 500g for 5 min at 4℃. Serum was collected and stored at − 80℃. Serum inflammatory factor concentrations were measured using a Mouse ELISA Kit in accordance with the manufacturer's instructions (Figure S1E).

Aortic ultrasound imaging

Abdominal aortas were visualized in isoflurane-anesthetized mice at the indicated endpoints using a color Doppler ultrasound system with ZS3 Exp Domain scanning imaging technique (Mindray, China). Cross-sectional images of the abdominal aorta were captured and the maximal lumen diameters at the aneurysm sites were measured. All measurements were made by two researchers in a blinded manner.

Neutrophil isolation and culture

Mice were sacrificed and bone marrow was removed. Neutrophils were isolated from the bone marrow using a mouse marrow neutrophil isolation kit (Solarbio, P8550). Immediately after isolation, the neutrophil layer was collected and resuspended in RPMI 1640 medium containing 5% fetal bovine serum and 1% penicillin/streptomycin. The cells were incubated at 37 ℃ and 5% CO2 in a humidified incubator and used for

NETosis studies after 30 min of isolation. The concentration of neutrophils was identified by staining and flow cytometry (Figure S3A-S3C).

Induction of NETs and interventions in vitro

Freshly purified neutrophils were grown on Poly-L-Lysine-coated coverslips in a 24-well plate. NETosis was inducted by different concentrations of lipopolysaccharide (LPS), with an optimal concentration of 5 μg/mL (Figure S3D). Neutrophils were treated with phosphate-buffered saline (PBS) as a negative control and LPS (5 μg/mL, Sigma–Aldrich) or tumor necrosis factor a (TNFa, 50 ng/mL, MedChemExpress) for 4 h to induce NET formation.

For NETosis, neutrophils were pretreated with IPI549 (5 μM, MedChemExpress) or disulfiram (DSF, 30 μM, MedChemExpress) for 1 h and then stimulated with LPS (5 μg/mL, Sigma–Aldrich) for 4 h to induce NET formation. In addition, to interfere with the reactive oxygen species (ROS) or Akt pathways, neutrophils were pretreated with diphenyleneiodonium chloride (DPI, 10 μM, MedChemExpress) or SC79 (4 μg/mL, MedChemExpress) for 1 h after IPI549 administration, and then stimulated with LPS for 4 h to induce NET formation.

To explore pyroptosis during NETosis, neutrophils were primed with ultrapure LPS (100 ng/mL) for 3 h, and then stimulated with nigericin (10 μM) for 1 h after IPI549 administration to induce canonical inflammasome activation. For noncanonical inflammasome activation, neutrophils were primed with Pam3CSK4 (1 μg/mL) for 3 h before IPI549 administration, and subsequently transfected without (Mock) or with

ultrapure LPS (10 μg/mL) into the cytosol using DOTAP Liposomal Transfection Reagent (Roche) for 4 h.

For cAMP/PKA inhibition, H89 (20 μM, MedChemExpress) or MDL12330A (10 μM, MedChemExpress) was added to neutrophils for 1 h after IPI549 administration, followed by stimulation with LPS for 4 h to induce NET formation.

After stimulation, cells were collected for subsequent test.

Immunohistochemistry

Aorta tissues were fixed in 4% paraformaldehyde (PFA), dehydrated in 70%-100% ethanol, embedded in paraffin and sectioned (5 μm). Antigen retrieval was performed using Sodium citrate-EDTA buffer in an autoclave for 6 min, followed by blocking nonspecific binding with 3% bovine serum albumin (BSA) containing 0.3% Triton X-100 for 1 h. Tissue sections were incubated with primary antibodies (see Table S1) overnight at 4℃. The sections were then rinsed and incubated with horseradish peroxidase (HRP)-conjugated secondary antibodies according to the manufacturer's protocol, and then stained with DAB (ZSGB-BIO, ZLI-9018) and hematoxylin. Images were obtained using a Leica DM6 M microscope (Leica Microsystems, Germany).

Immunofluorescence staining

Immunofluorescence staining before primary antibody incubation was carried out as for immunohistochemistry. Cells were fixed with 4% paraformaldehyde for 15 min, washed with PBS and permeabilized with 0.3% Triton X-100 for 10 min. After blocking

with 3% BSA for 1 h. Tissue sections or cells were incubated with primary antibodies overnight at 4℃ followed by corresponding fluorescent-conjugated secondary antibodies for 1 h at room temperature. The antibodies used are listed in Table S1. Images were obtained using Leica DMi8 M (Leica Microsystems). The cells were then stained with DAPI, citrullinated histone 3 (Cit H3) antibody and myeloperoxidase (MPO) antibody to detect NETs.

Verhoeff Van Gieson (VVG) staining

Aorta tissues were harvested, fixed with 4% PFA, paraffin embedded, and sectioned (5 μm). The sections were then processed for Verhoeff's elastic staining using a VVG Elastic Stain Kit (Abiowell, AWI0267b), according to the manufacturer's protocol. Images were obtained using a Leica DM6 M. The severity of elastin fragmentation was evaluated and graded as follows: grade 1, no degradation; grade 2, mild elastin degradation; grade 3, moderate elastin degradation; and grade 4, severe elastin degradation. Each sample was assessed by two independent pathologists.

Wright-Giemsa staining

Purified neutrophils were smeared and stained using Wright-Giemsa stain solution (Solarbio, G1020) in accordance with the manufacturer's instructions, and images were obtained using a Leica DM6 M.

Flow cytometry

Purified neutrophils were resuspended in cell staining buffer and 100 μL of cell suspension (1×10^6cells/tube) was then incubated with Zombie Aqua™ dye (BioLegend, 423101) for 20 min in the dark at room temperature. The cells were then washed with PBS and preincubated with 5 mL of TruStain FcX™ PLUS (anti-mouse CD16/32) antibody (Fc Receptor Blocking Solution, BioLegend, 156603) for 10 min on ice to reduce nonspecific immunofluorescent staining. The cell suspension was then incubated with FITC-conjugated fluorescent antibody against CD11b (BioLegend, 101205) and APC-conjugated fluorescent antibody against Ly6G (BioLegend, 127613) on ice for 20 min in the dark (Table S1). After washing twice with PBS, flow cytometry was conducted using a Cytek DxP Athena™ flow cytometer (Cytek Biosciences) and the data were analyzed using FlowJo 10 software.

cAMP concentration

cAMP concentrations in tissues and neutrophils were measured using a Mouse cAMP ELISA Kit (Jianglai Biotech, JL13362), in accordance with the manufacturer's instructions.

PKA activity

Purified neutrophil and tissue PKA activities were measured using a nonradioactive PKA Kinase Activity Assay Kit (Abcam, ab139435) following the manufacturer's instructions.

Quantitative Real-time polymerase chain reaction (PCR)

Total RNA was extracted using RNAiso Plus reagent (Takara, 9019) and reverse transcribed into cDNA using the Hifair® AdvanceFast One-step RT-gDNA Digestion SuperMix (Yeasen, 11151ES60). DNA was amplified under the following reaction conditions: denaturing at 95℃ for 3 min, followed by 40 cycles of annealing at 95℃ for 5 s and extension at 60℃ for 31 s in the presence of 2× Universal SYBR Green Fast qPCR Mix (Abclonal, RK21203) and primers. The PCR products were detected using an Applied Biosystems ViiA 7 Real-Time PCR System (ThermoFisher Scientific). Relative gene expression was determined by the $2^{-\Delta\Delta Ct}$ method. Primers were designed according to the coding sequences of the genes in the National Center for Biotechnology Information (NCBI) database and are listed in Table S3.

Western blot

Cleaved interleukin (IL)-1β in the cell supernatant was detected after purifying the proteins by the methanol–chloroform extraction method, as described previously (56). Briefly, neutrophil suspensions were centrifuged at 2000×g for 5 min, the cell supernatant was collected, and 500 μL methanol and 125 μL chloroform were added into 500 μL of supernatant and mixed vigorously. After centrifugation at 13,000 rpm for 5 min, the upper clear liquid was removed and 500 μL of methanol was added to the pellet to disperse it. Following another round of centrifugation at 13,000 rpm for 5 min, the white pellet was left to dry at 55°C for 10 min until no visible liquid was evident. Finally, 1× sodium dodecyl sulfate (SDS) loading buffer was added to the dry

proteins and heated for 5 min at 95°C, followed by immunoblotting analyses. For cell or tissue samples, proteins were isolated using RIPA buffer (Beyotime, P0013B) containing protease and phosphatase inhibitor (Beyotime, P1045) on ice, and their concentrations were determined using a BCA protein assay kit (Beyotime, P0012). After adding SDS-polyacrylamide gel (PAGE) protein loading buffer (Beyotime, P0015L) and denaturing at 95°C for 10 min, equal amounts of protein samples were separated in an SDS-PAGE gel and transferred to a polyvinylidene difluoride membrane. The membrane was blocked with 5% nonfat milk in TBST buffer for 1 h at room temperature and incubated with appropriate primary antibodies overnight at 4°C, followed by horseradish peroxidase-conjugated secondary antibody for 1 h at room temperature. The protein bands were visualized using an Immobilon Western HRP substrate Luminol Reagent (Millipore, WBKLS0500) and ChemiDoc XRS+ Imaging system (Bio-Rad). Densitometry analysis was performed using Image J software. The antibodies used in the present study are listed in Table S1.

Statistical analysis

Statistical analysis was performed using Prism 9.5 software (GraphPad Software, Inc.). Values are shown as mean ± standard deviation. Results were compared between two groups using Student's *t*-test and among multiple groups using one-way ANOVA Multiple groups with two variables were evaluated by two-way ANOVA followed by Bonferroni's test. Different interventions were compared among multiple groups using one-way ANOVA followed by Fisher's least significant difference *post hoc* test. For all

statistical methods, $P < 0.05$ were considered significance: *$P < 0.05$, **$P < 0.01$, ***$P < 0.001$.

Study approval

This study was approved by the Ethics Committee of Central South University Xiangya Hospital (Hunan province, China, Approval No.201803481) in accordance with the principles of the Declaration of Helsinki. All included subjects provided written informed consent. All animal procedures adhered to the US National Institutes of Health's Guide for the Care and Use of Laboratory Animals.

Data availability

The underlying data can be accessed in the "Supporting data values" XLS file.

Author contributions

BH. P., YQ. L., and W.W. designed the study and revised the paper. YC. X. performed experiments and wrote the paper. S.L., JN.Z., and JJ.S. helped with animal experiments. Y.L. contributed to sample collection.

Acknowledgments

This study was supported by the National Natural Science Foundation of China (NSFC, Grant No.81873525 and 82070491) and Youth Program of National Natural Science Foundation of China (Grant No.82202394). We thank Susan Furness, PhD, from Liwen Bianji (Edanz) (www.liwenbianji.cn), for editing the English text of a draft of this manuscript. We appreciate Peishan Ning, a statistician in Department of Epidemiology and Health Statistics, Xiangya School of Public Health, Central south university for valuable suggestion concerning statistical analysis.

Abbreviations

AAA: abdominal aortic aneurysm; Cit H3: citrullinated histones3; AC: adenylyl cyclase; CTA: computed tomography angiography; DSF: disulfiram; MMPs: matrix metalloproteinases; NETs: neutrophil extracellular traps; NOX2: nicotinamide adenine dinucleotide phosphate oxidase 2; PAD: peptidyl arginine deiminase; PDEs: phosphodiesterase; PI3Kγ: PI3Kgmma; PKA: protein kinase A; PPE: porcine pancreatic elastase; ROS: reactive oxygen species; SPF: specific pathogen-free; tLPS: transfected LPS.

Reference

1. J R Baman, et al. What Is an Abdominal Aortic Aneurysm? *Jama*. 2022; 328(22): 2280
2. P Song, et al. The Global and Regional Prevalence of Abdominal Aortic Aneurysms: A Systematic Review and Modelling Analysis. *Ann Surg*. 2022;
3. J M Guirguis-Blake, et al. Primary Care Screening for Abdominal Aortic Aneurysm: Updated Evidence Report and Systematic Review for the US Preventive Services Task Force. *Jama*. 2019; 322(22): 2219-2238
4. J Golledge, et al. Lack of an effective drug therapy for abdominal aortic aneurysm. *J Intern Med*. 2020; 288(1): 6-22
5. W Wang, et al. Hypoxia-inducible factor 1 in clinical and experimental aortic aneurysm disease. *J Vasc Surg*. 2018; 68(5): 1538-1550.e1532
6. Z Yuan, et al. Abdominal Aortic Aneurysm: Roles of Inflammatory Cells. *Front Immunol*. 2020; 11(609161
7. R A Quintana, et al. Cellular Mechanisms of Aortic Aneurysm Formation. *Circ Res*. 2019; 124(4): 607-618
8. J L Eliason, et al. Neutrophil depletion inhibits experimental abdominal aortic aneurysm formation. *Circulation*. 2005; 112(2): 232-240
9. R R Parikh, et al. Association of Differential Leukocyte Count With Incident Abdominal Aortic Aneurysm Over 22.5 Years: The ARIC Study. *Arterioscler Thromb Vasc Biol*. 2021; 41(8): 2342-2351
10. M B Pagano, et al. Critical role of dipeptidyl peptidase I in neutrophil recruitment

during the development of experimental abdominal aortic aneurysms. *Proc Natl Acad Sci U S A*. 2007; 104(8): 2855-2860

11. J Klopf, et al. Neutrophils as Regulators and Biomarkers of Cardiovascular Inflammation in the Context of Abdominal Aortic Aneurysms. *Biomedicines*. 2021; 9(9):
12. G Boivin, et al. Durable and controlled depletion of neutrophils in mice. *Nat Commun*. 2020; 11(1): 2762
13. V Poli, et al. Neutrophil intrinsic and extrinsic regulation of NETosis in health and disease. *Trends Microbiol*. 2022;
14. M Herre, et al. Neutrophil extracellular traps in the pathology of cancer and other inflammatory diseases. *Physiol Rev*. 2023; 103(1): 277-312
15. Q Remijsen, et al. Dying for a cause: NETosis, mechanisms behind an antimicrobial cell death modality. *Cell Death Differ*. 2011; 18(4): 581-588
16. W Eilenberg, et al. Histone citrullination as a novel biomarker and target to inhibit progression of abdominal aortic aneurysms. *Transl Res*. 2021; 233(32-46
17. S Yang, et al. Neutrophil extracellular traps induce abdominal aortic aneurysm formation by promoting the synthetic and proinflammatory smooth muscle cell phenotype via Hippo-YAP pathway. *Transl Res*. 2023; 255(85-96
18. M Spinosa, et al. Resolvin D1 decreases abdominal aortic aneurysm formation by inhibiting NETosis in a mouse model. *J Vasc Surg*. 2018; 68(6s): 93s-103s
19. E Plana, et al. Novel contributions of neutrophils in the pathogenesis of abdominal aortic aneurysm, the role of neutrophil extracellular traps: A systematic review.

Thromb Res. 2020; 194(200-208

20. A K Meher, et al. Novel Role of IL (Interleukin)-1β in Neutrophil Extracellular Trap Formation and Abdominal Aortic Aneurysms. *Arterioscler Thromb Vasc Biol*. 2018; 38(4): 843-853
21. X Liu, et al. PAD4 takes charge during neutrophil activation: Impact of PAD4 mediated NET formation on immune-mediated disease. *J Thromb Haemost*. 2021; 19(7): 1607-1617
22. P Li, et al. PAD4 is essential for antibacterial innate immunity mediated by neutrophil extracellular traps. *J Exp Med*. 2010; 207(9): 1853-1862
23. A C Márquez-Sánchez, et al. Immune and inflammatory mechanisms of abdominal aortic aneurysm. *Front Immunol*. 2022; 13(989933
24. J Zhu, et al. Targeting phosphatidylinositol 3-kinase gamma (PI3Kγ): Discovery and development of its selective inhibitors. *Med Res Rev*. 2021; 41(3): 1599-1621
25. T DeSouza-Vieira, et al. Neutrophil extracellular traps release induced by Leishmania: role of PI3Kγ, ERK, PI3Kσ, PKC, and [Ca2+]. *J Leukoc Biol*. 2016; 100(4): 801-810
26. H Kimura, et al. The effect and possible clinical efficacy of in vivo inhibition of neutrophil extracellular traps by blockade of PI3K-gamma on the pathogenesis of microscopic polyangiitis. *Mod Rheumatol*. 2018; 28(3): 530-541
27. H C Welch, et al. P-Rex1 regulates neutrophil function. *Curr Biol*. 2005; 15(20): 1867-1873
28. Y Tong, et al. Excessive neutrophil extracellular trap formation induced by

Porphyromonas gingivalis lipopolysaccharide exacerbates inflammatory responses in high glucose microenvironment. *Front Cell Infect Microbiol*. 2023; 13(1108228

29. F Chen, et al. Hesperetin attenuates sepsis-induced intestinal barrier injury by regulating neutrophil extracellular trap formation via the ROS/autophagy signaling pathway. *Food Funct*. 2023; 14(9): 4213-4227
30. G Sollberger, et al. Gasdermin D plays a vital role in the generation of neutrophil extracellular traps. *Sci Immunol*. 2018; 3(26):
31. B E Burdette, et al. Gasdermin D in pyroptosis. *Acta Pharm Sin B*. 2021; 11(9): 2768-2782
32. S M Lanahan, et al. The role of PI3Kγ in the immune system: new insights and translational implications. *Nat Rev Immunol*. 2022; 22(11): 687-700
33. A Perino, et al. Integrating cardiac PIP3 and cAMP signaling through a PKA anchoring function of p110γ. *Mol Cell*. 2011; 42(1): 84-95
34. M Wei, et al. Inhibition of Peptidyl Arginine Deiminase 4-Dependent Neutrophil Extracellular Trap Formation Reduces Angiotensin II-Induced Abdominal Aortic Aneurysm Rupture in Mice. *Front Cardiovasc Med*. 2021; 8(676612
35. K K Hannawa, et al. L-selectin-mediated neutrophil recruitment in experimental rodent aneurysm formation. *Circulation*. 2005; 112(2): 241-247
36. P Haider, et al. Neutrophil Extracellular Trap Degradation by Differently Polarized Macrophage Subsets. *Arterioscler Thromb Vasc Biol*. 2020; 40(9): 2265-2278
37. L Chen, et al. Mesenchymal stem cell-derived extracellular vesicles protect against

abdominal aortic aneurysm formation by inhibiting NET-induced ferroptosis. *Exp Mol Med*. 2023; 55(5): 939-951

38. D Song, et al. PTP1B inhibitors protect against acute lung injury and regulate CXCR4 signaling in neutrophils. *JCI Insight*. 2022; 7(14):
39. M M Kaneda, et al. PI3Kγ is a molecular switch that controls immune suppression. *Nature*. 2016; 539(7629): 437-442
40. A Lupieri, et al. Smooth muscle cells-derived CXCL10 prevents endothelial healing through PI3Kγ-dependent T cells response. *Cardiovasc Res*. 2020; 116(2): 438-449
41. J J Anzinger, et al. Murine bone marrow-derived macrophages differentiated with GM-CSF become foam cells by PI3Kγ-dependent fluid-phase pinocytosis of native LDL. *J Lipid Res*. 2012; 53(1): 34-42
42. V de Carvalho Oliveira, et al. Phosphoinositol 3-kinase-driven NET formation involves different isoforms and signaling partners depending on the stimulus. *Front Immunol*. 2023; 14(1042686
43. X Zhan, et al. Elevated neutrophil extracellular traps by HBV-mediated S100A9-TLR4/RAGE-ROS cascade facilitate the growth and metastasis of hepatocellular carcinoma. *Cancer Commun (Lond)*. 2023; 43(2): 225-245
44. X Lv, et al. Tetrachlorobenzoquinone exhibits immunotoxicity by inducing neutrophil extracellular traps through a mechanism involving ROS-JNK-NOX2 positive feedback loop. *Environ Pollut*. 2021; 268(Pt B): 115921
45. K W Chen, et al. Noncanonical inflammasome signaling elicits gasdermin D-

dependent neutrophil extracellular traps. *Sci Immunol*. 2018; 3(26):

46. J J Hu, et al. FDA-approved disulfiram inhibits pyroptosis by blocking gasdermin D pore formation. *Nat Immunol*. 2020; 21(7): 736-745

47. C M S Silva, et al. Gasdermin D inhibition prevents multiple organ dysfunction during sepsis by blocking NET formation. *Blood*. 2021; 138(25): 2702-2713

48. N Kayagaki, et al. Noncanonical inflammasome activation by intracellular LPS independent of TLR4. *Science*. 2013; 341(6151): 1246-1249

49. G Guo, et al. Neutrophil Function Conversion Driven by Immune Switchpoint Regulator against Diabetes-Related Biofilm Infections. *Adv Mater*. 2023; e2310320

50. E Patrucco, et al. PI3Kgamma modulates the cardiac response to chronic pressure overload by distinct kinase-dependent and -independent effects. *Cell*. 2004; 118(3): 375-387

51. A Ghigo, et al. Phosphoinositide 3-kinase γ protects against catecholamine-induced ventricular arrhythmia through protein kinase A-mediated regulation of distinct phosphodiesterases. *Circulation*. 2012; 126(17): 2073-2083

52. K D Puri, et al. The role of endothelial PI3Kgamma activity in neutrophil trafficking. *Blood*. 2005; 106(1): 150-157

53. M Yu, et al. Development and safety of PI3K inhibitors in cancer. *Arch Toxicol*. 2023; 97(3): 635-650

54. E L Chaikof, et al. The Society for Vascular Surgery practice guidelines on the care of patients with an abdominal aortic aneurysm. *J Vasc Surg*. 2018; 67(1): 2-77.e72

55. S Liu, et al. Spermidine Suppresses Development of Experimental Abdominal Aortic Aneurysms. *J Am Heart Assoc*. 2020; 9(8): e014757

56. C Jakobs, et al. Immunoblotting for active caspase-1. *Methods Mol Biol*. 2013; 1040(103-115

Figure legends

Figure 1. NETs are upregulated in both human and mouse AAA tissue

(A) Representative western blot image and quantitative analysis of Cit H3 protein expression in human AAA tissue and Adjacent AA tissue. n = 7.

(B) Representative western blot image and quantitative analysis of Cit H3 protein expression in mouse AAA tissue at different time points after PPE surgery. n = 3.

(C) Representative immunofluorescence staining images and quantitative comparison of NETs in human abdominal aortic sections. Nets expression was calculated by NET area/total area (%) according to the fluorescence colocalization of DNA (DAPI, Blue), Citrullinated histone 3 (Cit H3, Green), and Myeloperoxidase (MPO, red). n=6. Scale bars, 50μm.

(D) Representative immunofluorescence staining images and quantitative comparison of NETs in mouse abdominal aorta after PPE-induced AAA. Nets expression was calculated by NET area/total area (%) according to the fluorescence colocalization of DNA (DAPI, Blue), Citrullinated histone 3 (Cit H3, Green), and Myeloperoxidase (MPO, red). n=5 in control group and n=6 in AAA group. Scale bars, 50μm.

(A) Two-tailed paired student's t test. (B) One-way ANOVA followed by Dunnett's test. (C and D) Two-tailed unpaired student's t test.

*P<0.05, **P<0.01, and ***P<0.001. Adjacent AA, adjacent abdominal aorta; AAA, abdominal aortic aneurysm; Cit H3, citrullinated histone 3; PPE, Porcine pancreatic elastase; NETs, neutrophil extracellular traps.

Figure 2. Inhibition of NETs alleviates elastase-induced AAA in mice

(A) Schematic diagram of the animal study to verify the effect of Cl-amidine administration on PPE-induced AAA.

(B) Representative ultrasonic images and quantitative comparison of maximal lumen diameter in mouse abdominal aorta at different time points with various treatments. n=13 in Vehicle group and n=15 in Cl-amidine group. Scale bar: 1 mm

(C) Representative macroscopic images and quantitative comparison of maximal aortic diameter in mouse abdominal aorta at 14 days after PPE-induced AAA. n=11 in Vehicle group and n=9 in Cl-amidine group.

(D) Representative VVG staining images and quantitative comparison of mouse abdominal aorta in PPE-induced AAA. n = 6. Scale bars, 50 μm.

(E) Representative immunofluorescence staining images and quantitative comparison of NETs in mouse abdominal aorta after PPE-induced AAA. Nets expression was calculated by NET area/total area (%) according to the fluorescence colocalization of DNA (DAPI, Blue), Citrullinated histone 3 (Cit H3, Green), and Myeloperoxidase (MPO, red). n=6. Scale bars, 50μm.

(F) Representative western blot image and quantitative analysis of CitH3 protein expression in mouse AAA tissue at different time points with various treatment. n = 3.

(G) QPCR analysis of contractile, synthetic, inflammation, and matrix metalloproteinase genes expression normalized to the mean expression of housekeeping gene (*Actb*) in mouse abdominal aorta from vehicle and Cl-amidine administration after PPE-induced AAA. n=6.

(B and G) Two-way ANOVA followed by Bonferroni test. (C-F) Two-tailed unpaired

student's t test.

*P<0.05, **P<0.01, and ***P<0.001.PPE, Porcine pancreatic elastase; ip, intraperitoneal injection; NETs, neutrophil extracellular traps.

Figure 3. PI3Kγ knockout reduces neutrophil infiltration and NETs formation and improve AAA

(A) Representative ultrasonic images and quantitative comparison of maximal lumen diameter in mouse abdominal aorta at different time points after PPE-induced AAA. n=13. Scale bar: 1 mm

(B) Representative macroscopic images and quantitative comparison of maximal aortic diameter in mouse abdominal aorta at 14 days after PPE-induced AAA. n=11 in wild type (WT) group and n=9 in *PI3Kγ*$^{-/-}$ group.

(C) Representative immunohistochemistry staining images and quantitative comparison of neutrophil infiltration in mouse abdominal aorta after PPE-induced AAA. Neutrophil infiltration was assessed by Ly6G+ neutrophil numbers per high-power field (40X). n=6. Scale bars, 50 μm.

(D) Representative immunofluorescence staining images and quantitative comparison of NETs in mouse abdominal aorta after PPE-induced AAA. Nets expression was calculated by NET area/total area (%) according to the fluorescence colocalization of DNA (DAPI, Blue), Citrullinated histone 3 (Cit H3, Green), and Myeloperoxidase (MPO, red). n=6. Scale bars, 50 μm.

(E) Representative western blot image and quantitative analysis of Cit H3 protein

expression in mouse AAA tissue at different time points after PPE surgery. n = 3.

(A) Two-way ANOVA followed by Bonferroni test. (B-E) Two-tailed unpaired student's t test.

*P<0.05, **P<0.01, and ***P<0.001.PPE, WT, wide type; *PI3Kγ*$^{-/-}$, phosphoinositide 3-kinase γ knockout; NETs, neutrophil extracellular traps.

Figure 4. Deficiency of PI3Kγ inhibits NETs formation in neutrophil

(A and C) Representative immunofluorescence staining images and quantitative comparison of NETs produced by neutrophils with different treatments: PBS (WT-derived neutrophils), LPS (5 μg/mL, WT-derived neutrophils), LPS (*PI3Kγ*$^{-/-}$ derived neutrophil); PBS (WT-derived neutrophils), TNFa (50 ng/mL, WT-derived neutrophils), TNFa (*PI3Kγ*$^{-/-}$ derived neutrophil). NETs were detected using immunofluorescent staining of DNA (DAPI, blue), Citrullinated histone 3 (Cit H3, Green), and Myeloperoxidase (MPO, red). NETs expression was calculated by NETs cell numbers/total cell numbers per high-power field (40X). n=6. Scale bars, 50 μm.

(B and D) Representative western blot images and quantitative comparison of Cit H3 protein expression in each group of neutrophils with different treatments as described in (A) or (C). n=3.

(A-D) One-way ANOVA followed by Fisher's LSD post hoc test.

*P<0.05, **P<0.01, and ***P<0.001.PBS, phosphate buffered saline; LPS, Lipopolysaccharide; TNFa, tumor necrosis factor alpha; NETs, neutrophil extracellular traps.

Figure 5. PI3Kγ expression in neutrophil is required for NETs formation and AAA progression in mice

(A) Schematic diagram of the experimental process of neutrophil adoptive transfer in PPE-induced AAA *PI3Kγ*$^{-/-}$ mice.

(B) Representative ultrasonic images (D) and quantitative comparison (E) of maximal lumen diameter in PI3Kγ-/- mice after PPE surgery. n=8. Scale bar: 1 mm.

(C) Representative macroscopic images and quantitative comparison of maximal aortic diameter in *PI3Kγ*$^{-/-}$- mice after PPE surgery. n=8.

(D) Representative VVG staining images and quantitative comparison of VVG staining score in *PI3Kγ*$^{-/-}$ mice after PPE surgery. n = 6. Scale bars, 50 μm.

(E) Representative immunofluorescence staining images and quantitative comparison of NETs in *PI3Kγ*$^{-/-}$ mice abdominal aorta after PPE-induced AAA. Nets expression was calculated by NET area/total area (%) according to the fluorescence colocalization of DNA (DAPI, Blue), Citrullinated histone 3 (Cit H3, Green), and Myeloperoxidase (MPO, red). n=6. Scale bars, 50 μm.

(F) Representative western blot image and quantitative analysis of Cit H3 protein expression in the abdominal aorta of *PI3Kγ*$^{-/-}$ mice. n = 3.

(G) QPCR analysis of contractile, synthetic, inflammation, and matrix metalloproteinase genes expression normalized to the mean expression of housekeeping gene (*Actb*) in abdominal aorta of *PI3Kγ*$^{-/-}$ mice from control and WT neutrophil adoptive transfer after PPE-induced AAA. n=6.

(B-F) Two-tailed unpaired student's t test. (G) Two-way ANOVA followed by Bonferroni test.

*P<0.05, **P<0.01, and ***P<0.001. WT, wide type; *PI3Kγ*$^{-/-}$, phosphoinositide 3-kinase γ knockout; iv, intravenous injection; NETs, neutrophil extracellular traps.

Figure 6. PI3Kγ promotes NETs formation via noncanonical pyroptosis pathways in vitro.

(A) Representative western blot (A) and quantitative comparison of Cit H3 and GSDMD in WT neutrophils with different treatments: PBS, LPS (5μg/mL), and LPS + Disulfiram (30μM). n=3.

(B) Representative western blot and quantitative comparison of IL-1β and GSDMD in neutrophils with different treatments: PBS, LPS (5μg/mL), LPS + KO (*PI3Kγ*$^{-/-}$). n=3.

(C) Representative western blot and quantitative comparison of Cit H3, IL-1β, GSDMD, Caspase11, and Caspase1 in the neutrophils with different treatments: PBS, LPS (100ng/mL), LPS + Nigericin (10μM), LPS + Nigericin + KO; PBS, Pam3CSK4 (1μg/mL), Pam3CSK4 + tLPS (10μg/mL, transfer LPS), Pam3CSK4 + tLPS + KO. n=3.

(D) Representative immunofluorescence staining and quantitative comparison of NETs produced by neutrophils with different treatments: PBS, LPS (5μg/mL), LPS + KO, LPS + H89 (20μM) + KO, LPS + MDL12330A (10μM) + KO. NETs were detected using immunofluorescent staining. NETs expression was calculated by NETs cell numbers/total cell numbers per high-power field (40X). n=6. Scale bars, 50 μm.

(E) Comparison of cAMP concentration of neutrophil with different treatments as described in (D) by Elisa Kit. n=4.

(F) Comparison of PKA kinase activity of neutrophil with different treatments as described in (D) by kinase activity assay Kit. n=4.

(G) Representative western blot and quantitative comparison of Cit H3, GSDMD, and Caspase11 in the neutrophils with different treatments as described in (M). n=3.

(A-G) One-way ANOVA followed by Fisher's LSD post hoc test.

*P<0.05, **P<0.01, and ***P<0.001. Cit H3, citrullinated histone 3; GSDMD, Gasdermin D; pro-, prosoma; cle-, cleaved; IL-1β, interleukin 1 beta; Casp1, caspase 1; Casp11, caspase11; LPS, Lipopolysaccharide; DSF, disulfiram; Nig, nigericin; Pam, Pam3CSK4; tLPS, transfer Lipopolysaccharide; KO, phosphoinositide 3-kinase γ knockout; MDL, MDL12330A; cAMP, cyclic adenosine monophosphate; PKA, protein kinase A.

Figure 7. cAMP/PKA inhibitor eliminates protective effect of PI3Kγ knockout in elastase-induced AAA

(A) Schematic diagram of the animal study to verify the effect of H89 administration in PPE-induced AAA *PI3Kγ*$^{-/-}$ mice.

(B) Representative ultrasonic images and quantitative comparison of maximal lumen diameter in PI3Kγ-/- mice after PPE surgery. n=8. Scale bar: 1 mm.

(C) Representative macroscopic images and quantitative comparison of maximal aortic diameter in PI3Kγ-/- mice after PPE surgery. n=8.

(D) Representative VVG staining images and quantitative comparison of VVG staining score in *PI3Kγ*$^{-/-}$ mice after PPE surgery. n = 6. Scale bars, 50 μm.

(E) QPCR analysis of contractile, synthetic, inflammation, and matrix metalloproteinase genes expression normalized to the mean expression of housekeeping gene (*Actb*) in abdominal aorta of *PI3Kγ*$^{-/-}$ mice from vehicle and H89 administration after PPE-induced AAA. n=6.

(F and G) The concentration of cAMP (F) and PKA activity (G) in the abdominal aorta of *PI3Kγ*$^{-/-}$ mice. n = 6.

(H) Representative western blot image and quantitative analysis of Cit H3, GSDMD, and Caspase11 protein expression in the abdominal aorta of *PI3Kγ*$^{-/-}$ mice. n = 3.

(I) Representative immunofluorescence staining images and quantitative comparison of NETs in *PI3Kγ*$^{-/-}$ mice abdominal aorta after PPE-induced AAA. Nets expression was calculated by NET area/total area (%) according to the fluorescence colocalization of DNA (DAPI, Blue), Citrullinated histone 3 (Cit H3, Green), and Myeloperoxidase (MPO, red). n=6. Scale bars, 50 μm

(B-D and F-I) Two-tailed unpaired student's t test. (E) Two-way ANOVA followed by Bonferroni test.

**P*<0.05, ***P*<0.01, and ****P*<0.001. PPE, Porcine pancreatic elastase; Cit H3, citrullinated histone 3; GSDMD, Gasdermin D; pro-, prosoma; cle-, cleaved; Casp11, caspase11; *PI3Kγ*$^{-/-}$, phosphoinositide 3-kinase γ knockout; MDL, MDL12330A; cAMP, cyclic adenosine monophosphate; PKA, protein kinase A; NETs, neutrophil extracellular traps.

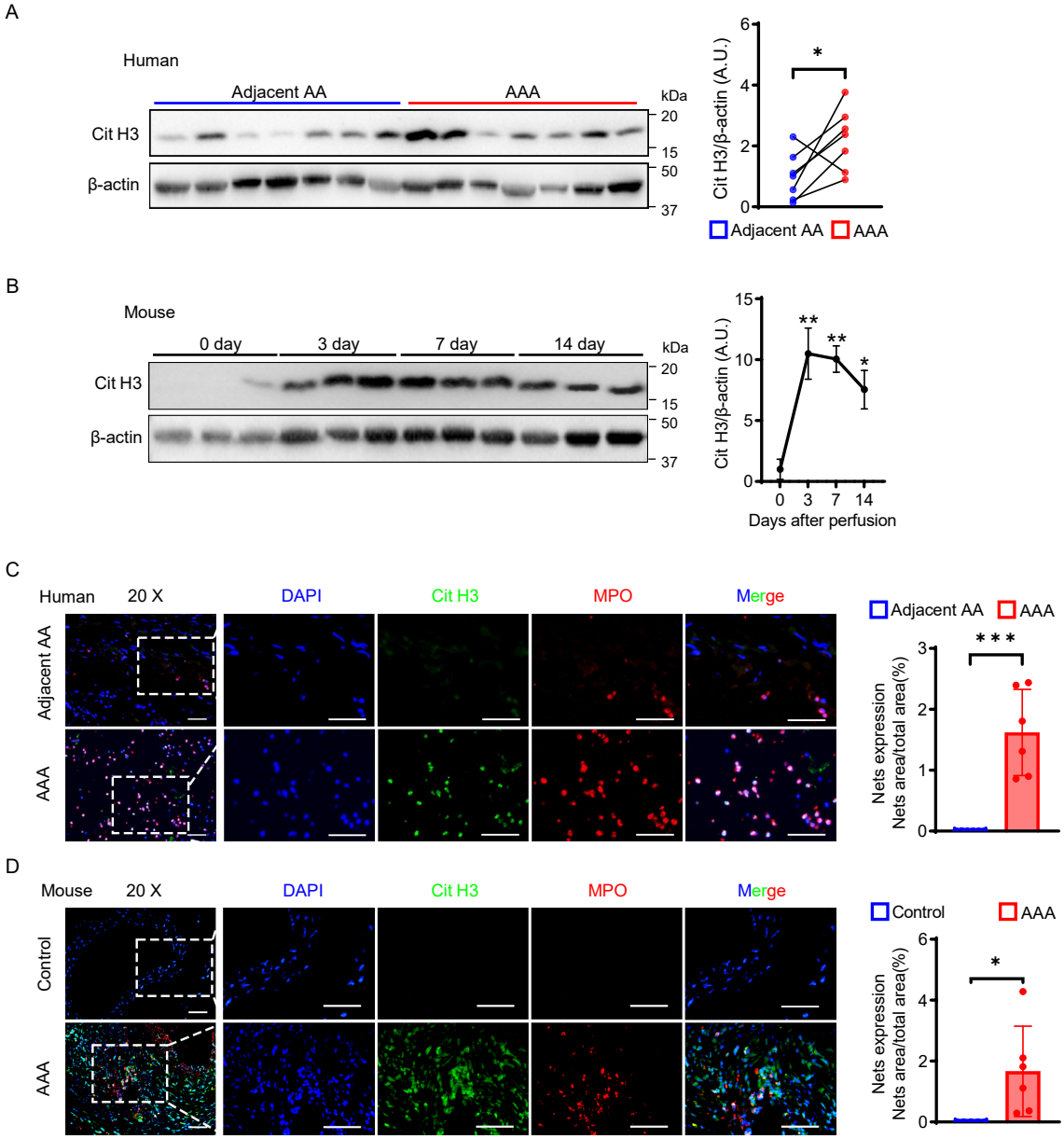
A
Human
Adjacent AA
AAA
kDa
Cit H3
β-actin
20
15
50
37
Cit H3/β-actin (A.U.)
*
Adjacent AA
AAA
B
Mouse
0 day
3 day
7 day
14 day
kDa
Cit H3
β-actin
20
15
50
37
Cit H3/β-actin (A.U.)
**
**
*
Days after perfusion
C
Human
20 X
DAPI
Cit H3
MPO
Merge
Adjacent AA
AAA
Adjacent AA
AAA
***
Nets expression
Nets area/total area(%)
D
Mouse
20 X
DAPI
Cit H3
MPO
Merge
Control
AAA
Control
AAA
*
Nets expression
Nets area/total area(%)

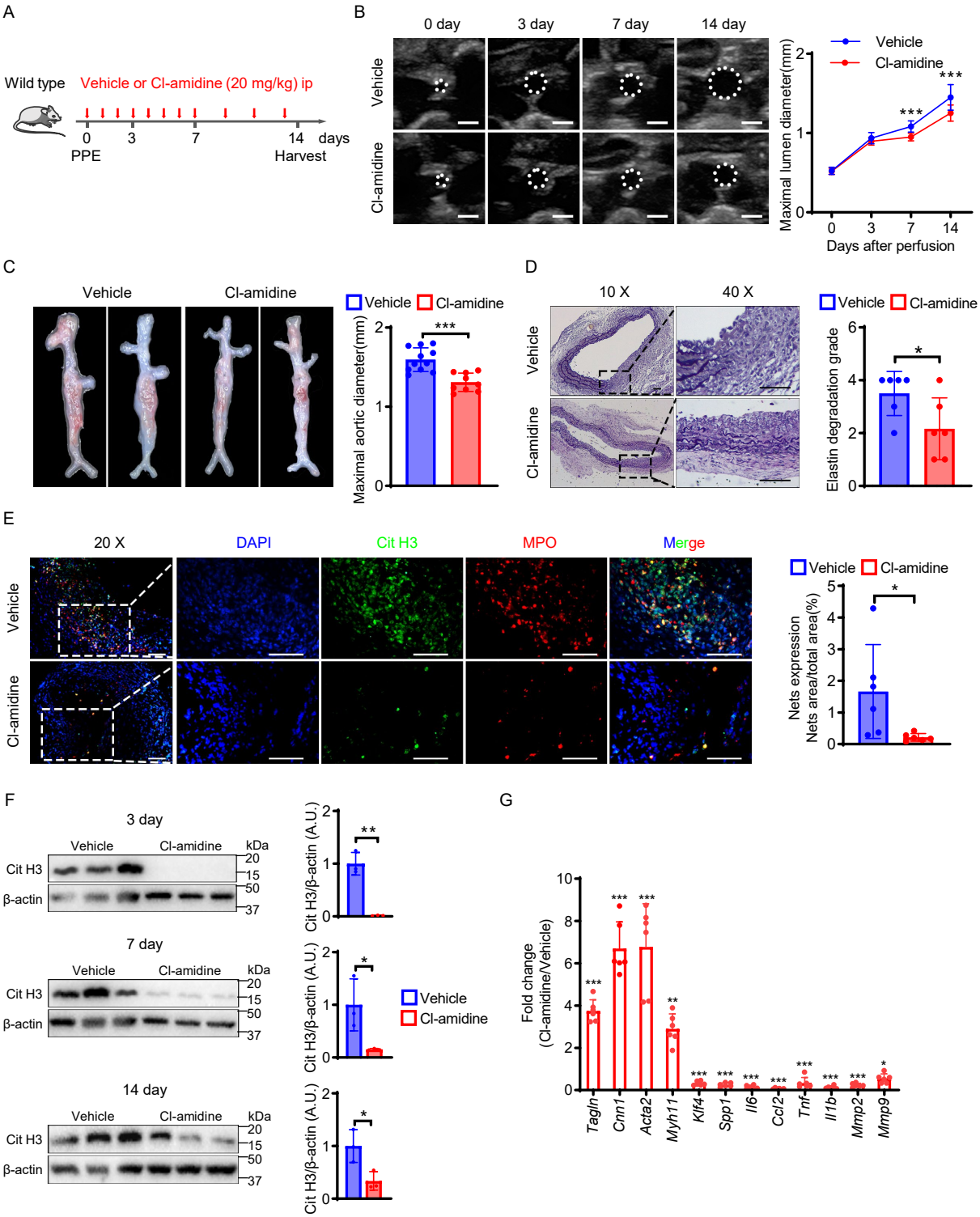
A
Wild type
Vehicle or Cl-amidine (20 mg/kg) ip
0
3
7
14
days
PPE
Harvest
B
0 day
3 day
7 day
14 day
Vehicle
Cl-amidine
Maximal lumen diameter(mm)
Days after perfusion
C
Vehicle
Cl-amidine
Maximal aortic diameter(mm)
D
10 X
40 X
Elastin degradation grade
E
20 X
DAPI
Cit H3
MPO
Merge
Nets expression
Nets area/total area(%)
F
3 day
7 day
14 day
kDa
Cit H3
β-actin
Cit H3/β-actin (A.U.)
G
Fold change
(Cl-amidine/Vehicle)
Tagln
Cnn1
Acta2
Myh11
Klf4
Spp1
Il6
Ccl2
Tnf
Il1b
Mmp2
Mmp9

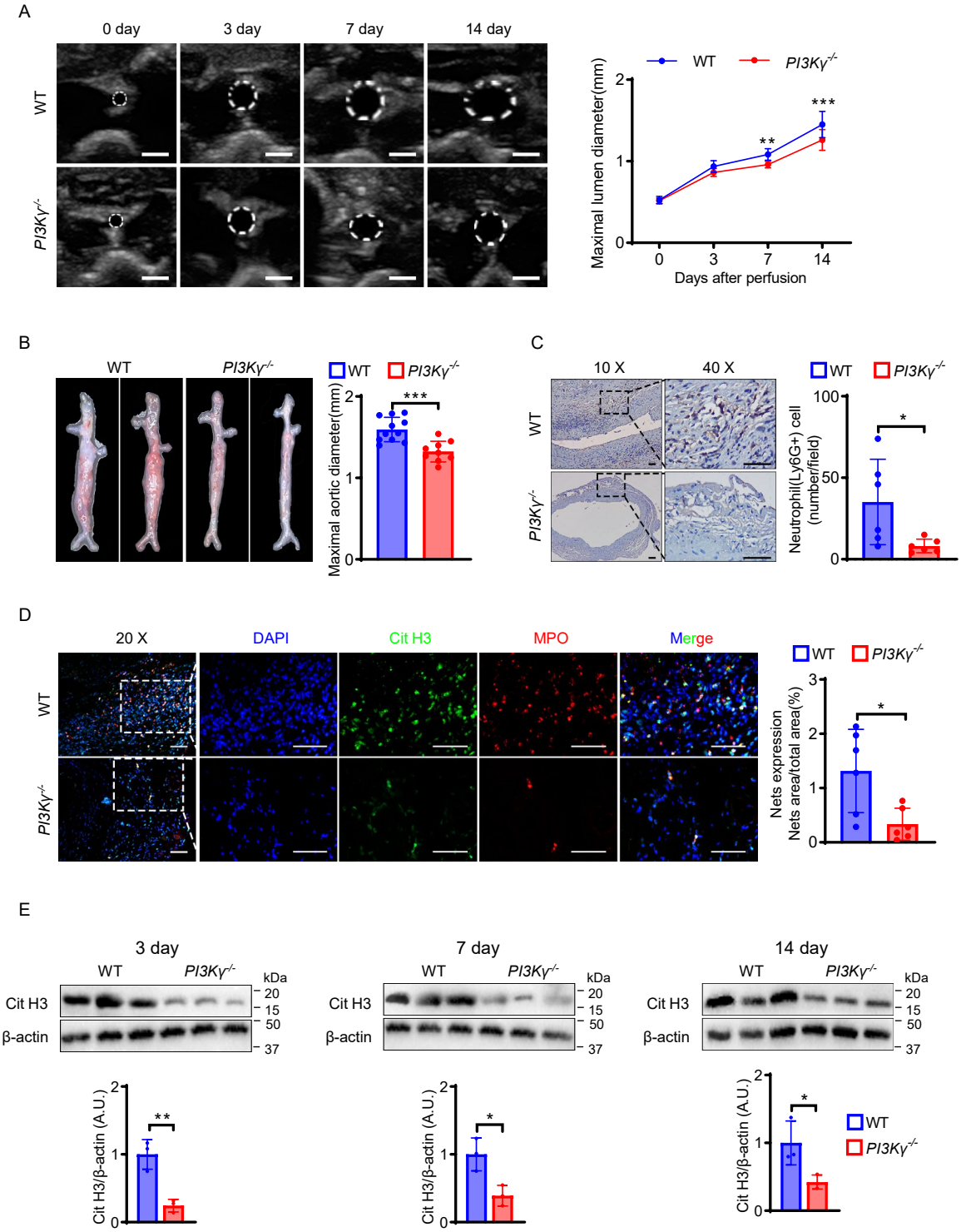
A
0 day
3 day
7 day
14 day
WT
PI3Kγ-/-
Maximal lumen diameter(mm)
Days after perfusion
B
Maximal aortic diameter(mm)
C
10 X
40 X
Neutrophil(Ly6G+) cell (number/field)
D
20 X
DAPI
Cit H3
MPO
Merge
Nets expression Nets area/total area(%)
E
3 day
7 day
14 day
kDa
Cit H3
β-actin
Cit H3/β-actin (A.U.)

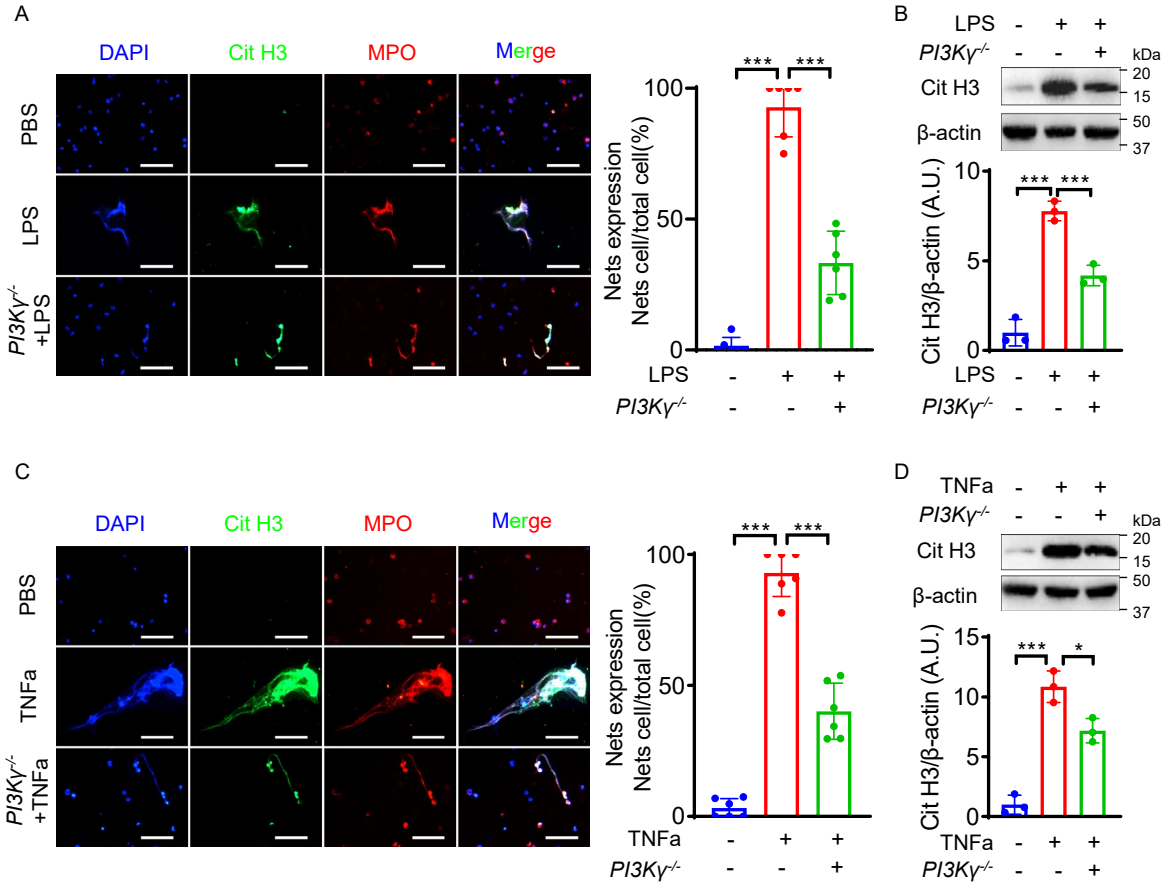
A
DAPI
Cit H3
MPO
Merge
PBS
LPS
PI3Kγ-/- +LPS
Nets expression
Nets cell/total cell(%)
100
50
0
***
***
LPS - + +
PI3Kγ-/- - - +
B
LPS - + +
PI3Kγ-/- - - +
kDa
Cit H3
β-actin
20
15
50
37
Cit H3/β-actin (A.U.)
10
5
0
***
***
LPS - + +
PI3Kγ-/- - - +
C
DAPI
Cit H3
MPO
Merge
PBS
TNFa
PI3Kγ-/- +TNFa
Nets expression
Nets cell/total cell(%)
100
50
0
***
***
TNFa - + +
PI3Kγ-/- - - +
D
TNFa - + +
PI3Kγ-/- - - +
kDa
Cit H3
β-actin
20
15
50
37
Cit H3/β-actin (A.U.)
15
10
5
0
***
*
TNFa - + +
PI3Kγ-/- - - +

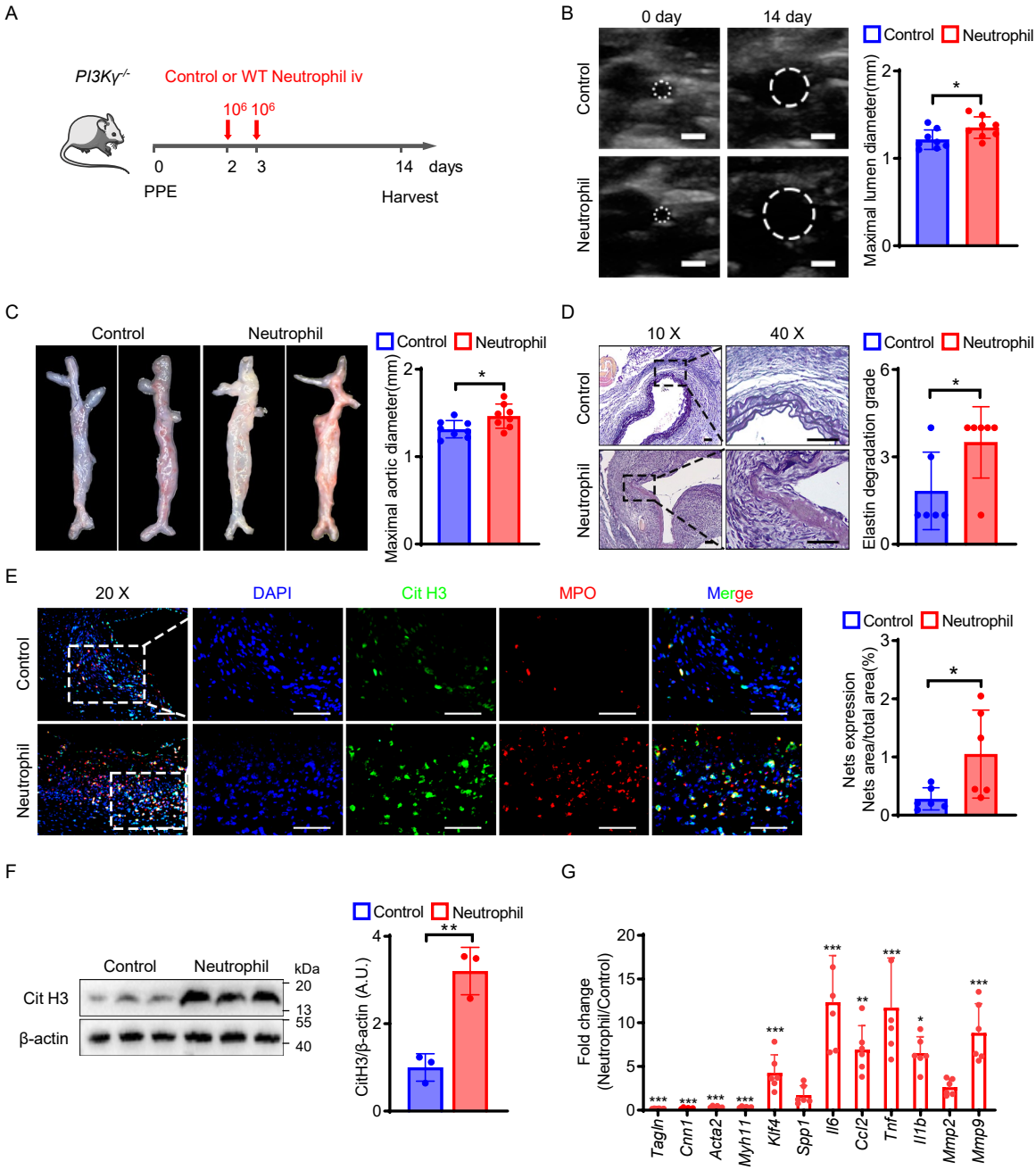
A
PI3Kγ-/-
Control or WT Neutrophil iv
10^6 10^6
0
2
3
14
days
PPE
Harvest
B
0 day
14 day
Control
Neutrophil
Maximal lumen diameter(mm)
C
Control
Neutrophil
Maximal aortic diameter(mm)
D
10 X
40 X
Elastin degradation grade
E
20 X
DAPI
Cit H3
MPO
Merge
Nets expression
Nets area/total area(%)
F
Cit H3
β-actin
kDa
20
13
55
40
CitH3/β-actin (A.U.)
G
Fold change
(Neutrophil/Control)
Tagln
Cnn1
Acta2
Myh11
Klf4
Spp1
Il6
Ccl2
Tnf
Il1b
Mmp2
Mmp9

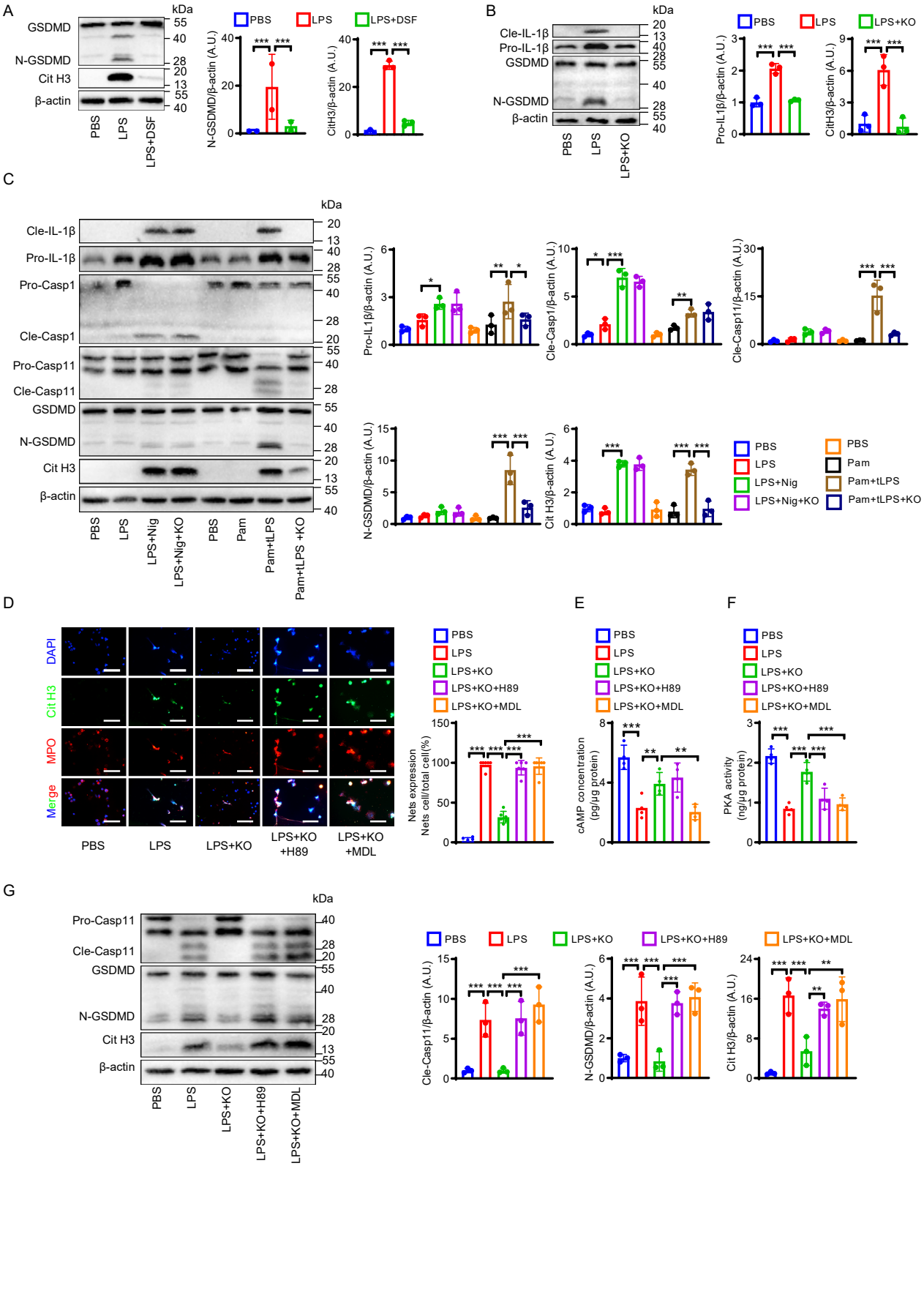
A
kDa
GSDMD
N-GSDMD
Cit H3
β-actin
PBS
LPS
LPS+DSF
N-GSDMD/β-actin (A.U.)
CitH3/β-actin (A.U.)
B
Cle-IL-1β
Pro-IL-1β
LPS+KO
Pro-IL1β/β-actin (A.U.)
C
Pro-Casp1
Cle-Casp1
Pro-Casp11
Cle-Casp11
LPS+Nig
LPS+Nig+KO
Pam
Pam+tLPS
Pam+tLPS +KO
Pro-IL1β/β-actin (A.U.)
Cle-Casp1/β-actin (A.U.)
Cle-Casp11/β-actin (A.U.)
Cit H3/β-actin (A.U.)
LPS+Nig
LPS+Nig+KO
Pam
Pam+tLPS
Pam+tLPS+KO
D
DAPI
Cit H3
MPO
Merge
LPS+KO
LPS+KO +H89
LPS+KO +MDL
Nets expression
Nets cell/total cell(%)
E
cAMP concentration (pg/μg protein)
F
PKA activity (ng/μg protein)
LPS+KO+H89
LPS+KO+MDL
G
Cle-Casp11/β-actin (A.U.)

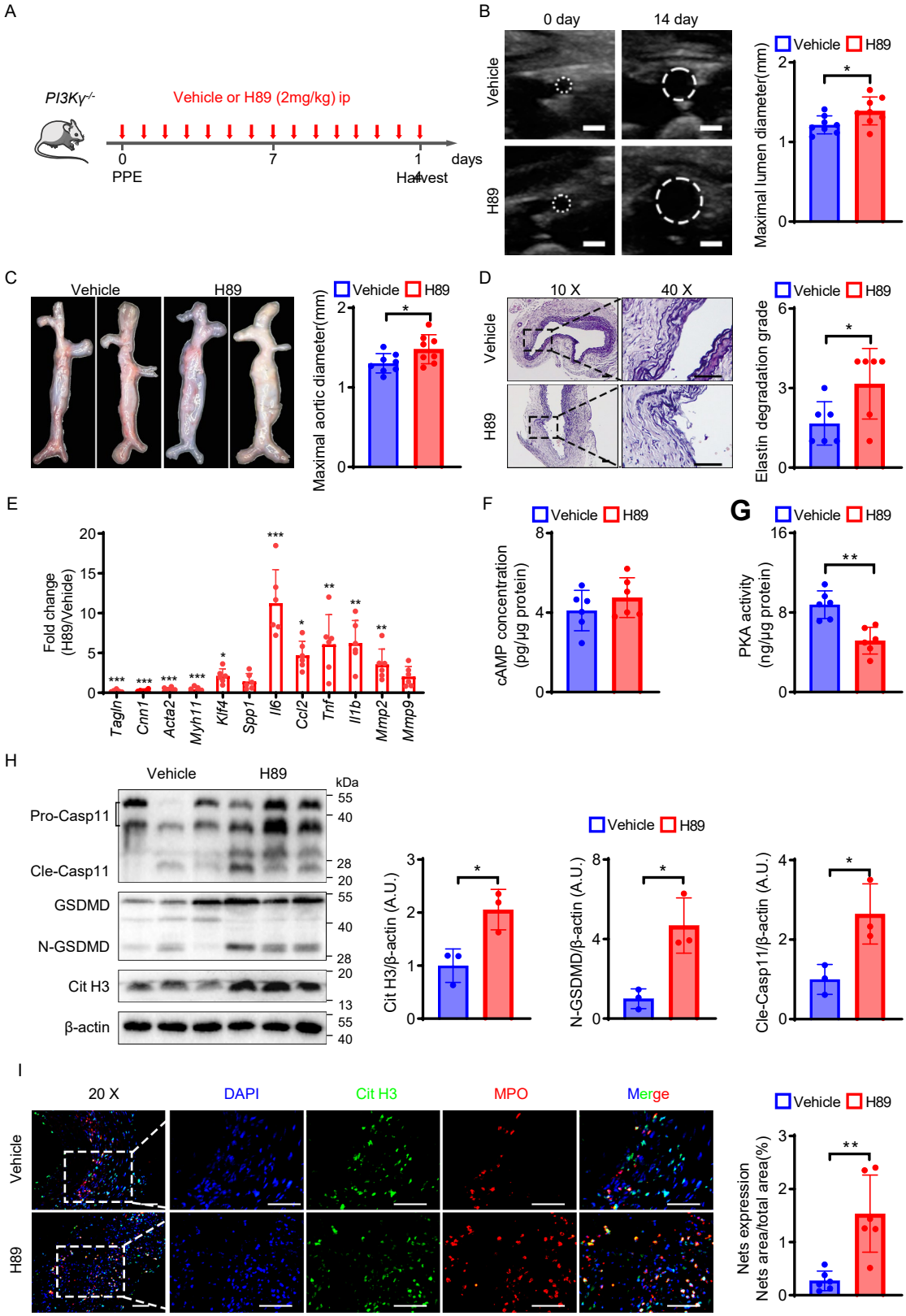
A
PI3Kγ-/-
Vehicle or H89 (2mg/kg) ip
0
PPE
7
1
Harvest
days
B
0 day
14 day
Vehicle
H89
Maximal lumen diameter(mm)
C
Vehicle
H89
Maximal aortic diameter(mm)
D
10 X
40 X
Elastin degradation grade
E
Fold change (H89/Vehicle)
Tagln
Cnn1
Acta2
Myh11
Klf4
Spp1
Il6
Ccl2
Tnf
Il1b
Mmp2
Mmp9
F
cAMP concentration (pg/μg protein)
G
PKA activity (ng/μg protein)
H
kDa
Pro-Casp11
Cle-Casp11
GSDMD
N-GSDMD
Cit H3
β-actin
Cit H3/β-actin (A.U.)
N-GSDMD/β-actin (A.U.)
Cle-Casp11/β-actin (A.U.)
I
20 X
DAPI
Cit H3
MPO
Merge
Nets expression
Nets area/total area(%)